

# Measurement of underlying event characteristics using charged particles in $pp$ collisions at $\sqrt{s} = 900$ GeV and 7 TeV with the ATLAS detector

G. Aad *et al.*\*

(The ATLAS Collaboration)

(Dated: October 22, 2018)

## Abstract

Measurements of charged particle distributions, sensitive to the underlying event, have been performed with the ATLAS detector at the LHC. The measurements are based on data collected using a minimum-bias trigger to select proton–proton collisions at center-of-mass energies of 900 GeV and 7 TeV. The “underlying event” is defined as those aspects of a hadronic interaction attributed not to the hard scattering process, but rather to the accompanying interactions of the rest of the proton. Three regions are defined in azimuthal angle with respect to the highest transverse momentum charged particle in the event, such that the region transverse to the dominant momentum-flow is most sensitive to the underlying event. In each of these regions, distributions of the charged particle multiplicity, transverse momentum density, and average  $p_T$  are measured. The data show generally higher underlying event activity than that predicted by Monte Carlo models tuned to pre-LHC data.

---

\* Full author list given at the end of the article in Appendix ??.

## I. INTRODUCTION

To perform precise Standard Model measurements or search for new physics phenomena at hadron colliders, it is essential to have a good understanding not only of the short-distance “hard” scattering process, but also of the accompanying interactions of the rest of the proton – collectively termed the “underlying event” (UE). It is impossible to uniquely separate the UE from the hard scattering process on an event-by-event basis. However, observables can be measured which are sensitive to its properties.

The UE may involve contributions from both hard and soft physics, where “soft” refers to interactions with low  $p_T$  transfer between the scattering particles. Soft interactions cannot reliably be calculated with perturbative QCD methods, and are generally described in the context of different phenomenological models, usually implemented in Monte Carlo (MC) event generators. These models contain many parameters whose values are not *a priori* known. Therefore, to obtain insight into the nature of soft QCD processes and to optimize the description of UE contributions for studies of hard-process physics such as hadronic jet observables, the model parameters must be fitted to experimental data.

Measurements of primary charged particle multiplicities have been performed in “minimum bias” (MB) events at the LHC [1–5]. Such inclusive studies provide important constraints on soft hadron-interaction models. However, observables constructed for the study of the UE measure the structure of hadronic events in a different way, focusing on the correlation of soft-process features to one another and to those of the hardest processes in the event. UE observables have been measured in  $p\bar{p}$  collisions in dijet and Drell-Yan events at CDF in Run I [6] and Run II [7] at center-of-mass energies of  $\sqrt{s} = 1.8$  TeV and 1.96 TeV respectively, and in  $pp$  collisions at  $\sqrt{s} = 900$  GeV in a detector-specific study by CMS [8].

This paper reports the measurement of UE observables, performed with the ATLAS detector [9] at the LHC using proton–proton collisions at center-of-mass energies of 900 GeV and 7 TeV. The UE observables are constructed from primary charged particles in the pseudorapidity range  $|\eta| < 2.5$ , whose transverse momentum component [10] is separately required to be  $p_T > 100$  MeV or  $p_T > 500$  MeV. Primary charged particles are defined as those with a mean proper lifetime  $\tau \gtrsim 0.3 \times 10^{-10}$  s, either directly produced in  $pp$  interactions or in the decay of particles with a shorter lifetime. At the detector level, charged particles are observed as tracks in the inner tracking system. The direction of the track with

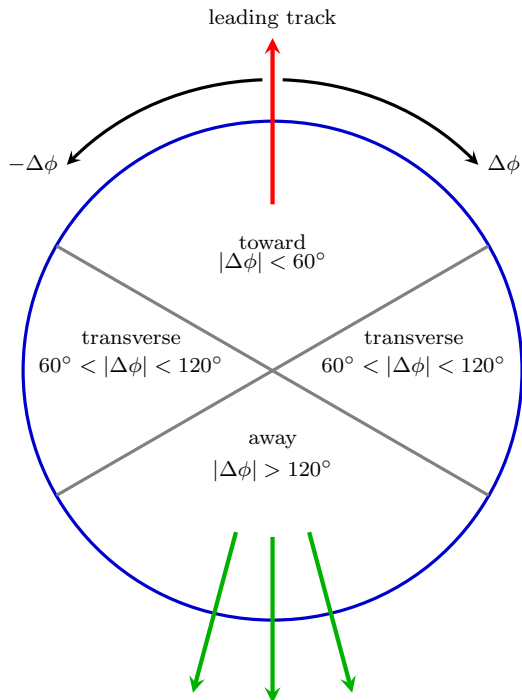


FIG. 1. Definition of regions in the azimuthal angle with respect to the leading track.

the largest  $p_T$  in the event – referred to as the “leading” track – is used to define regions of the  $\eta$ – $\phi$  plane which have different sensitivities to the UE. The axis given by the leading track is well-defined for all events, and is highly correlated with the axis of the hard scattering in high- $p_T$  events. A single track is used as opposed to a jet or the decay products of a massive gauge boson, as it allows significant results to be derived with limited luminosity and avoids the systematic measurement complexities of alignment with more complex objects.

As illustrated in Fig. 1, the azimuthal angular difference between charged tracks and the leading track,  $|\Delta\phi| = |\phi - \phi_{\text{leading track}}|$ , is used to define the following three azimuthal regions [6]:

- $|\Delta\phi| < 60^\circ$ , the “toward region”;
- $60^\circ < |\Delta\phi| < 120^\circ$ , the “transverse region”; and
- $|\Delta\phi| > 120^\circ$ , the “away region”.

The transverse regions are most sensitive to the underlying event, since they are generally perpendicular to the axis of hardest scattering and hence have the lowest level of activity from this source. However, the hard scatter can of course also emit particles perpendicular

to the event axis: the regional division is not, and cannot be, an exact filter. The observables examined in this analysis are described in Table I. The detector level corresponds to the tracks passing the selection criteria, and the particle level corresponds to true charged particles in the event. The particle level can be compared directly with the QCD Monte Carlo models at the generator level.

This paper is organized as follows: The ATLAS detector is described in Section II. In Section III, the QCD MC models used in this analysis are discussed. Sections IV–VII respectively describe the event selection, background contributions, correction of the data back to particle level, and estimation of the systematic uncertainties. The results are discussed in Section VIII and finally the conclusions are presented in Section IX.

## II. THE ATLAS DETECTOR

The ATLAS detector [9] covers almost the whole solid angle around the collision point with layers of tracking detectors, calorimeters and muon chambers. It has been designed to study a wide range of physics topics at LHC energies. For the measurements presented in this paper, the trigger system and the tracking devices were of particular importance.

The ATLAS inner detector has full coverage in  $\phi$  and covers the pseudorapidity range  $|\eta| < 2.5$ . It consists of a silicon pixel detector (pixel), a silicon strip detector namely the semiconductor tracker (SCT) and a straw-tube transition radiation tracker (TRT). These detectors cover a radial distance from the interaction point of 50.5–150 mm, 299–560 mm and 563–1066 mm, respectively, and are immersed in a 2 Tesla axial magnetic field. The inner detector barrel (end-cap) parts consist of 3 ( $2 \times 3$ ) pixel layers, 4 ( $2 \times 9$ ) layers of double-sided silicon strip modules, and 73 ( $2 \times 160$ ) layers of TRT straw-tubes. These detectors have position resolutions of typically 10, 17 and 130  $\mu\text{m}$  for the  $r$ - $\phi$  coordinate and (for the pixel and SCT) 115 and 580  $\mu\text{m}$  for the  $r$ - $z$  coordinate. A track traversing the barrel would typically have 11 silicon hits (3 pixel clusters, and 8 strip clusters), and more than 30 straw-tube hits.

The ATLAS detector has a three-level trigger system: level 1 (L1), level 2 (L2) and the event filter (EF). For this measurement, the trigger relies on the beam pickup timing devices (BPTX) and the minimum bias trigger scintillators (MBTS). The BPTX are composed of electrostatic beam pick-ups attached to the beam pipe at a distance  $z = \pm 175$  m from the

TABLE I. Definition of the measured observables at particle and detector level. The particles and tracks are required to have  $p_T > 0.1$  GeV or 0.5 GeV and  $|\eta| < 2.5$ . Tracks are selected if they pass the criteria described in Section IV. The mean charged particle momentum  $\langle p_T \rangle$  is constructed on an event-by-event basis and then averaged over the events.

Observable	Particle level	Detector level
$p_T^{\text{lead}}$	Transverse momentum of the stable charged particle with maximum $p_T$ in the event	Transverse momentum of the selected track with maximum $p_T$ in the event
$ \eta ^{\text{lead}}$	$ \eta $ of the maximum $p_T$ stable charged particle in the event	$ \eta $ of the maximum $p_T$ selected track in the event
$\langle d^2 N_{\text{ch}}/d\eta d\phi \rangle$	Mean number of stable charged particles per unit $\eta-\phi$	Mean number of selected tracks per unit $\eta-\phi$
$\langle d^2 \sum p_T/d\eta d\phi \rangle$	Mean scalar $p_T$ sum of stable charged particles per unit $\eta-\phi$	Mean scalar $p_T$ sum of selected tracks per unit $\eta-\phi$
Standard deviation of $d^2 N_{\text{ch}}/d\eta d\phi$	Standard deviation of number of stable charged particles per unit $\eta-\phi$	Standard deviation of number of selected tracks per unit $\eta-\phi$
Standard deviation of $d^2 \sum p_T/d\eta d\phi$	Standard deviation of scalar $p_T$ sum of stable charged particles per unit $\eta-\phi$	Standard deviation of scalar $p_T$ sum of selected tracks per unit $\eta-\phi$
$\langle p_T \rangle$	Average $p_T$ of stable charged particles (at least 1 charged particle is required)	Average $p_T$ of selected tracks (at least 1 selected track is required)
Angular distribution of number density	Number density of stable charged particles in intervals of $\Delta \phi $ , measured relative to the leading charged particle	Number density of tracks in intervals of $\Delta \phi $ , measured relative to the leading track
Angular distribution of $p_T$ density	$p_T$ density of stable charged particles in the intervals of $\Delta \phi $ , measured relative to the leading charged particle	$p_T$ density of tracks in the intervals of $\Delta \phi $ , measured relative to the leading track

center of the ATLAS detector. The MBTS are mounted at each end of the detector in front of the liquid-argon endcap-calorimeter cryostats at  $z = \pm 3.56$  m and are segmented into eight sectors in azimuth and two rings in pseudorapidity ( $2.09 < |\eta| < 2.82$  and  $2.82 < |\eta| < 3.84$ ). Data were taken for this analysis using the single-arm MBTS trigger, formed from BPTX and MBTS trigger signals. The MBTS trigger was configured to require one hit above threshold from either side of the detector. The MBTS trigger efficiency was studied with a separate pre-scaled L1 BPTX trigger, filtered to obtain inelastic interactions by inner detector requirements at L2 and EF.

### III. QCD MONTE CARLO MODELS

In scattering processes modeled by lowest-order perturbative QCD two-to-two parton scatterers, at sufficiently low  $p_T$  the partonic jet cross-section exceeds that of the total hadronic cross-section. This problem is resolved by allowing the possibility of multiple parton interactions (MPI) in a given hadron-hadron interaction. In this picture, the ratio of the partonic jet cross-section to the total cross-section is interpreted as the mean number of parton interactions in such events. This idea is implemented in several Monte Carlo event generators, and is usually complemented by phenomenological models which continue to be developed. These include (non-exhaustively) further low  $p_T$  screening of the partonic differential cross-section, use of phenomenological transverse hadronic-matter distributions, reconfiguration of color string or cluster topologies, saturation of parton densities at low- $x$ , and connection to elastic scattering and cut-pomeron models via the optical theorem. Such models typically contain several parameters, which may be tuned to data at different center-of-mass energies and in various hadronic processes. MC tuning has been actively pursued in recent years, and standard tunes are being iterated in response to early LHC data, including those presented in ref. [5].

Samples of 10–20 million MC events were produced for single-diffractive, double-diffractive and non-diffractive processes using the PYTHIA 6.4.21 generator [11] for collision energies of 900 GeV and 7 TeV. The MC09 [12] set of Tevatron-optimized parameters was used: this employs the MRST LO\* [13] parton density functions (PDFs) [14] and the PYTHIA  $p_T$ -ordered parton shower, and was tuned to describe underlying event and minimum bias data at 630 GeV and 1.8 TeV [15] at CDF in  $p\bar{p}$  collisions. ATLAS MC09 is the reference

PYTHIA tune throughout this paper, and samples generated with this tune were used to calculate detector acceptances and efficiencies to correct the data for detector effects. All events were processed through the ATLAS detector simulation framework [16], which is based on Geant4 [17]. They were then reconstructed and analyzed identically to the data. Particular attention was devoted to the description in the simulation of the size and position of the collision beam-spot and of the detailed detector conditions during the data-taking runs.

For the purpose of comparing the present measurement to different phenomenological models, several additional MC samples were generated. For PYTHIA, these were the Perugia0 [18] tune, in which the soft-QCD part of the event is tuned using only minimum bias data from the Tevatron and  $S\bar{p}p$ S colliders, and the DW [19] PYTHIA tune, which uses a virtuality-ordered parton shower and an eikonal multiple scattering model including impact-parameter correlations. This tune was constructed to describe CDF Run II underlying event, dijet and Drell-Yan data. PHOJET [20] and HERWIG [21] were used as alternative models. PHOJET describes low- $p_T$  physics using the two component Dual Parton Model [22, 23], which includes soft hadronic processes described by pomeron exchange and semi-hard processes described by perturbative parton scattering; it relies on PYTHIA for the fragmentation of partons. The PHOJET versions used for this study were shown to agree with previous measurements [15, 24–26]. The PHOJET samples were also passed through full detector simulation for systematic studies of acceptance and smearing corrections (unfolding). HERWIG uses angular-ordered parton showers and a cluster hadronization model. The UE is simulated using the JIMMY package [27] which, like PYTHIA, implements an eikonal multiple scattering model including impact-parameter correlations. It does not contain any model of soft scatters. HERWIG+JIMMY was run with the ATLAS MC09 parameters [12]: these set a minimum partonic interaction  $p_T$  of 3.0 GeV at 900 GeV and 5.2 GeV at 7 TeV, and hence agreement with data is not expected when the maximum track  $p_T$  is below this cut-off scale.

For PYTHIA and PHOJET, non-diffractive, single-diffractive and double-diffractive events were generated separately, and were mixed according to the generator cross-sections to fully describe the inelastic scattering. HERWIG does not contain any diffractive processes.

#### IV. EVENT AND TRACK SELECTION

All data used in this paper were taken during the LHC running periods with stable beams and defined beam-spot values, between 6th–15th December 2009 for the analysis at  $\sqrt{s} = 900$  GeV, and from 30th March to 27th April 2010 for the 7 TeV analysis. The only operational requirement was that the MBTS trigger and all inner detector subsystems were at nominal conditions. During the December data taking period, more than 96% of the pixel detector, more than 99% of the SCT and more than 98% of the TRT was operational. These efficiencies were higher in 2010.

To reduce the contribution from backgrounds and secondaries, as well as to minimize the systematic uncertainties, the following criteria were imposed:

- the presence of a reconstructed primary vertex using at least two tracks, each with:
  - $p_T > 100$  MeV;
  - offline reconstruction within the inner detector,  $|\eta| < 2.5$ ;
  - a transverse distance of closest approach with respect to the beam-spot (BS) position,  $|d_0^{BS}|$ , of less than 4 mm;
  - uncertainties on the transverse and longitudinal distances of closest approach of  $\sigma(d_0^{BS}) < 5$  mm and  $\sigma(z_0^{BS}) < 10$  mm;
  - at least one pixel hit, at least four SCT hits and at least six silicon hits in total.

Beam-spot information was used both in the track pre-selection and to constrain the fit during iterative vertex reconstruction, and vertices incompatible with the beam-spot were removed. The vertices were ordered by the  $\sum p_T^2$  over the tracks assigned to the vertex, which is strongly correlated with the total number of associated tracks, with the highest- $\sum p_T^2$  vertex defined as the primary interaction vertex of the event.

Events that had a second primary vertex with more than three tracks in the same bunch crossing were rejected. If the second vertex had three or fewer tracks, all tracks from the event that passed the selection were kept. After this cut, the fraction of events with more than one interaction in the same bunch crossing (referred to as pile-up) was found to be about 0.1%; the residual effect was thus neglected. At  $\sqrt{s} = 900$  GeV,



since the data were taken at the low luminosity period, the rate of pileup was even lower and was also neglected.

- at least one track with:
  - $p_T > 1$  GeV,
  - a minimum of one pixel and six SCT hits[28];
  - a hit in the innermost pixel layer (the b-layer), if the corresponding pixel module was active;
  - transverse and weighted-longitudinal impact parameters with respect to the event-by-event primary vertex were required to be  $|d_0| < 1.5$  mm and  $|z_0| \cdot \sin \theta < 1.5$  mm [29];
  - for tracks with  $p_T > 10$  GeV, a  $\chi^2$  probability of track fit  $> 0.01$  was required in order to remove mismeasured tracks[30].

Only events with leading track  $p_T > 1$  GeV were considered, in order to reject events where the leading track selection can potentially introduce large systematic effects. This also has the effect of further reducing the contribution from diffractive scattering processes.

Two separate analyses were performed, in which all the other tracks were required to have either  $p_T > 100$  MeV or  $p_T > 500$  MeV. For  $p_T > 500$  MeV tracks, the silicon and impact parameter requirements were the same as given earlier for tracks with  $p_T > 1$  GeV. For tracks with the lower  $p_T$  threshold, all other selection criteria were the same except that only two, four or six SCT hits were required for tracks with  $p_T \geq 100, 200, 300$  MeV, respectively. Tracks with  $p_T > 500$  MeV are less prone than lower- $p_T$  tracks to inefficiencies and systematic uncertainties resulting from interactions with the material inside the tracking volume. Whenever possible, the tracks were extrapolated to include hits in the TRT. Typically, 88% of tracks inside the TRT acceptance ( $|\eta| < 2.0$ ) included a TRT extension, which significantly improves the momentum resolution.

After these selections, for the 500 MeV (100 MeV) analysis, 189,164 and 6,927,129 events remained at 900 GeV and 7 TeV respectively, containing 1,478,900 (4,527,710) and 89,868,306 (209,118,594) selected tracks and corresponding to integrated luminosities of  $7 \mu\text{b}^{-1}$  and  $168 \mu\text{b}^{-1}$ , respectively. For the MC models considered here, the contribution of diffractive events to the underlying event observables was less than 1%.

## V. BACKGROUND CONTRIBUTIONS

### A. Backgrounds

The amount of beam and non-beam (cosmic rays and detector noise) background remaining after the full event selection was estimated using the number of pixel hits which were not associated to a reconstructed track. This multiplicity included unassigned hits from low- $p_T$  looping tracks, but was dominated at higher multiplicities by hits from charged particles produced in beam background interactions. The vertex requirement removed most of the beam background events and the residual contribution from beam background events after this requirement was below 0.1%. As the level of background was found to be very low, no explicit background subtraction was performed.

### B. Fraction of secondary tracks

The primary charged-particle multiplicities were measured from selected tracks after correcting for the fractions of secondary and poorly reconstructed tracks in the sample. The potential background from fake tracks was found via MC studies to be less than 0.01%.

Non-primary tracks predominantly arise from hadronic interactions, photon conversions to positron-electron pairs, and decays of long-lived particles. For  $p_T$  above 500 MeV the contribution from photon conversions is small, and side-band regions of the transverse and longitudinal impact parameters from data were used to find a scaling factor of 1.3 for the track yield in MC to get a better agreement with the data. This is not the case at lower  $p_T$ . A separate fit to the tails of the  $d_0$  distribution for primaries, non-primaries from electrons and other non-primaries, was carried out in eight bins of 50 MeV in the range  $100 < p_T < 500$  MeV. The scaled MC was then used to estimate the fraction of secondaries as a function of both  $p_T$  and  $\eta$  in the selected track sample, which is found to be at most 2% for events in both 900 GeV and 7 TeV collisions [4, 5]. The systematic uncertainty on the secondaries is included in the uncertainties due to tracking.

## VI. CORRECTION TO PARTICLE LEVEL

The data were corrected back to charged primary particle spectra satisfying the event-level requirement of at least one primary charged particle within  $p_T > 1$  GeV and  $|\eta| < 2.5$ . A two step correction process was used, where first the event and track efficiency corrections were applied, then an additional bin-by-bin unfolding was performed to account for possible bin migrations and any remaining detector effects.

### A. Event-level correction

Trigger and vertexing efficiencies were measured [5] as a function of the number of tracks,  $N_{\text{sel}}^{\text{BS}}$ , passing all the track selection requirements except for the primary vertex constraint. In this case the transverse impact parameter with respect to the beam-spot [31] was required to be less than 1.8 mm. The event level corrections consisted of the following:

- The efficiency of the MBTS scintillator trigger,  $\epsilon_{\text{trig}}(N_{\text{sel}}^{\text{BS}})$  was determined from data using an orthogonal trigger. It consisted of a random trigger, requiring only that the event coincided with colliding bunches and had at least 4 pixel clusters and at least 4 SCT space points at L2. The trigger was found to be  $\sim 97\%$  efficient for low-multiplicity events, and almost fully efficient otherwise. It showed no dependence on the  $p_T$  and pseudorapidity distributions of the selected tracks.
- The vertex reconstruction efficiency,  $\epsilon_{\text{vtx}}(N_{\text{sel}}^{\text{BS}}, \langle \eta \rangle)$  was also measured in data, by taking the ratio of the number of triggered events with a reconstructed vertex to the total number of triggered events. For events containing fewer than three selected tracks, the efficiency was found to depend on the projected separation along the beam axis of the two extrapolated tracks,  $\Delta z_0^{\text{BS}}$ . This efficiency amounted to approximately 90% for the lowest bin of  $N_{\text{sel}}^{\text{BS}}$ , rapidly rising to 100%.
- A correction factor,  $\epsilon_{\text{ld trk}}(\epsilon_{\text{trk}})$  accounts for the probability that due to the tracking inefficiency none of the candidate leading tracks with  $p_T > 1$  GeV are reconstructed in an event, resulting in the event failing the selection criteria. A partial correction for this was provided by determining the probability that all possible reconstructed leading tracks would be missed for each event using the known tracking efficiencies, and

then dividing the event weight by this probability. This process will in general yield an excessive correction, since the correct weight should be determined using the number and distributions of true charged particles with  $p_T > 1$  GeV and  $|\eta| < 2.5$  rather than the distributions of reconstructed tracks. This leads to an over-estimation of the probability for the event to be omitted. Nevertheless, this correction represents a good estimate of the efficiency, given the efficiency estimate of tracks in each event. The efficiency was found to be  $> 98\%$  in low- $p_T$  bins and almost  $100\%$  in high- $p_T$  bins. The uncertainty for this correction is included as part of the tracking efficiency systematic uncertainty. The correction was made with the expectation that the final unfolding in the form of bin-by-bin corrections will provide the small additional correction that is needed.

The total correction applied to account for events lost due to the trigger, vertex, and tracking requirements (in bins of number of tracks with  $p_T > 0.5$  GeV) is given by

$$w_{\text{ev}} = \frac{1}{\epsilon_{\text{trig}}(N_{\text{sel}}^{\text{BS}})} \cdot \frac{1}{\epsilon_{\text{vtx}}(N_{\text{sel}}^{\text{BS}}, \langle \eta \rangle)} \cdot \frac{1}{\epsilon_{\text{ld trk}}(\epsilon_{\text{trk}})}, \quad (1)$$

where  $\epsilon_{\text{trig}}(N_{\text{sel}}^{\text{BS}})$ ,  $\epsilon_{\text{vtx}}(N_{\text{sel}}^{\text{BS}}, \langle \eta \rangle)$  and  $\epsilon_{\text{ld trk}}(\epsilon_{\text{trk}})$  are the trigger, vertex reconstruction and leading track reconstruction efficiencies discussed earlier.

## B. Track-level correction

The track-reconstruction efficiency in each bin of the  $p_T$ - $\eta$  kinematic plane, was determined from simulation and defined as

$$\epsilon_{\text{bin}}(p_T, \eta) = \frac{N_{\text{rec}}^{\text{matched}}(p_T, \eta)}{N_{\text{gen}}(p_T, \eta)}, \quad (2)$$

where  $N_{\text{rec}}^{\text{matched}}(p_T, \eta)$  is the number of reconstructed tracks in a given bin matched to a generated charged particle, and  $N_{\text{gen}}(p_T, \eta)$  is the number of generated particles in that bin. The matching between a generated particle and a reconstructed track was done using a cone-matching algorithm in the  $\eta$ - $\phi$  plane and associating the particle to the track with the smallest  $R = \sqrt{(\Delta\phi)^2 + (\Delta\eta)^2}$  within a cone of radius  $\Delta R < 0.15$ . To reduce fake matching, a common pixel hit between the reconstructed, simulated track and the generated particle

track in the Geant4 simulation was also required. The efficiencies were slightly different between the datasets at the two different center-of-mass energies because of small differences in the configuration of the pixel and SCT detectors between the 2009 and 2010 data-taking periods.

A weight,

$$w_{\text{trk}} = \frac{1}{\epsilon_{\text{bin}}(p_{\text{T}}, \eta)} \cdot (1 - f_{\text{sec}}(p_{\text{T}})) \cdot (1 - f_{\text{fake}}), \quad (3)$$

was applied on a track-by-track basis to all track-level histograms. Here  $\epsilon_{\text{bin}}(p_{\text{T}}, \eta)$  is the track-reconstruction efficiency described earlier,  $f_{\text{sec}}$  is the fraction of secondaries, and  $f_{\text{fake}}$  is the fraction of fakes.

### C. Final unfolding step

The efficiency corrections described so far do not account for bin-by-bin migrations, nor for the possibility of not reconstructing the leading particle in the event as the leading track (reorientation of an event). To account for these effects, an additional bin-by-bin unfolding was applied to all distributions after applying the event- and track-level efficiency corrections described above.

In this correction step, the unfolding factors were evaluated separately in each bin for each observable listed in Table I,

$$U_{\text{bin}} = \frac{V_{\text{bin}}^{\text{Gen}}}{V_{\text{bin}}^{\text{Reco, eff corr}}}, \quad (4)$$

where  $V_{\text{bin}}^{\text{Gen}}$  and  $V_{\text{bin}}^{\text{Reco, eff corr}}$  respectively represent the generator level MC value of the observable and the reconstructed MC value after applying the event- and track-level efficiency corrections at each bin. The corrected value for an observable is found by multiplying the measured value by the corresponding unfolding factor. This unfolding factor is within 5% (10%) of unity in the lowest- $p_{\text{T}}$  bins for the  $p_{\text{T}} > 100$  MeV (500 MeV) analyses respectively, due to the migration and reorientation effects, and very close to unity for higher- $p_{\text{T}}$  bins.

## VII. SYSTEMATIC UNCERTAINTIES

A study of the systematic uncertainties was performed, and these were propagated to the final distributions and added in quadrature to obtain a total systematic uncertainty.

Systematic uncertainties from tracking efficiency were studied [4, 5], and the largest were found to be due to the following:

- The material in the inner detector: the effect of material budget uncertainties in the inner detector was determined to affect the efficiency by a relative difference of 2% in the barrel region, rising to over 7% for  $2.3 < |\eta| < 2.5$ , for tracks with  $p_T > 500$  MeV.
- Consequence of  $\chi^2$  probability cut: the maximum difference between the fraction of events in data and MC which passed this cut was found to be 10%. This value was taken as a conservative estimate of the systematic uncertainty, applied to tracks with  $p_T > 10$  GeV only.

The systematic uncertainty from pile-up removal was estimated to be negligible.

The most common UE observable is a “profile” plot of the mean value of a charged particle  $p_T$  or multiplicity observable as a function of the  $p_T$  of the leading object in the event. Due to the steeply-falling  $p_T$  spectrum in minimum bias events, the number of events in the low- $p_T$  bins of these profiles is much higher than in the higher- $p_T$  bins, and so migration of the leading track from the lower- $p_T$  bins to higher ones is possible: this was accounted for in the MC-based unfolding procedure. However, an additional systematic uncertainty was included because more  $p_T^{\text{lead}}$  migrations are expected in data than in the MC detector modelling. This extra systematic contributes only to the region of the profiles with  $p_T^{\text{lead}} > 10$  GeV, since a small fraction of highly mismeasured leading tracks from the lowest  $p_T^{\text{lead}}$  bin can still have a significant effect upon the less-populated high- $p_T^{\text{lead}}$  bins. Since the greatest difference from the  $p_T^{\text{lead}}$ -profile values in  $p_T^{\text{lead}} > 10$  GeV is seen in the first  $p_T^{\text{lead}}$  bin, a conservative systematic estimate was obtained by assuming all migrations to come from the first bin.

The remaining contributions to the overall systematic uncertainty result from the specific unfolding method used in this analysis. The bin-by-bin unfolding corrections are in general influenced by the number of charged particles and their  $p_T$  distributions, so there is some dependence on the event generator model. This introduces a second extra source of systematic uncertainty. In order to estimate this uncertainty it is necessary to compare different

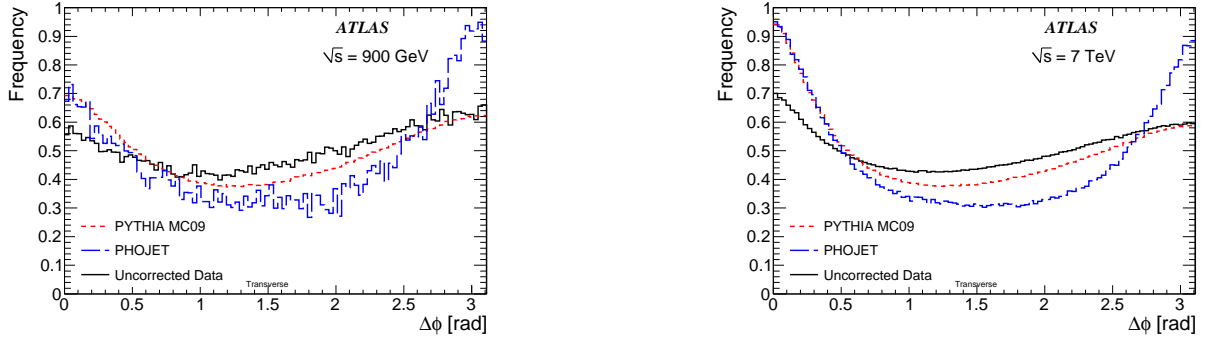


FIG. 2. Difference in  $\phi$  between the leading and the sub-leading track in PYTHIA, PHOJET and in uncorrected data. The left plot is for 900 GeV and the right is for 7 TeV. The MC curves are shown after the full detector simulation.

plausible event generation models, which deviate significantly from each other. Between the various models and tunes already described, the maximal variation is seen between PYTHIA and PHOJET, and this difference is taken as a measure of the uncertainty due to model-dependence. Where the PHOJET sample has sufficient statistics, it is seen that beyond the statistical fluctuations the relative difference between the required correction factors from PHOJET and PYTHIA are at most 4% in the lowest- $p_T$  bins, and 2% everywhere else.

Since this uncertainty is independent of any efficiency systematics, it has been summed in quadrature with the efficiency systematic uncertainty and the statistical uncertainty. In addition to the model-dependent uncertainty in the bin-by-bin unfolding, there is also a statistical uncertainty due to the finite size of the Monte Carlo sample. The statistical fluctuation of the PYTHIA unfolding factor is found to be negligible for low- $p_T$  bins, but rises to be a significant contribution in higher  $p_T$  bins.

The  $|\Delta\phi|$  between the leading track and the track with the second-highest  $p_T$  (the sub-leading track) is shown in Fig. 2. It is seen to be most likely that the sub-leading charged particle lies in either the true toward or the true away region, in which case there is relatively little effect on the observables – the transverse region is particularly unaffected by a  $\sim 180^\circ$  reorientation. However, if the reconstructed leading track lies in what should have been the transverse region, the effect will be to reduce the densities in the toward and away regions, and to increase the densities in the transverse region. The bin-by-bin unfolding derived from the MC corrects for this effect, provided that it occurs with the frequency of reorientation predicted by the MC simulation. Fig. 2 is used to estimate the relative frequency with which

an event is reoriented such that the true towards and away regions lie in the transverse region identified by the reconstruction. Comparing the  $|\Delta\phi|$  distribution in uncorrected data to the same distributions (uncorrected and reconstructed) predicted by PYTHIA and PHOJET, it is seen that both generator models predict fewer event reorientations of this type. The final correction to the data uses bin-by-bin unfolding factors that are derived from the PYTHIA sample, so the relative magnitude of the systematic uncertainty associated with this effect can again be estimated by the difference of the PYTHIA and PHOJET probabilities. This difference is comparable with the difference between the data and PYTHIA predictions. The uncertainty is applied in both directions, reasonably assuming a symmetric effect, so the difference in PYTHIA and PHOJET corrections provides the systematic uncertainty in the unfolding factor even though the PHOJET deviation from PYTHIA is in the opposite direction from the data.

Table II summarizes the various contributions to the systematic uncertainties.

TABLE II. Summary of systematic uncertainties, shown for the lowest-, intermediate- and highest- $p_T$  bins. For the analysis with 7 TeV (900 GeV) center-of-mass energy data, the lowest- $p_T$  bin refers to  $p_T^{\text{lead}} = 1.0 - 1.5$  GeV, the intermediate  $p_T$  bin refers to  $p_T^{\text{lead}} = 9 - 10$  GeV (4 - 5 GeV), and the highest  $p_T$  bin refers to  $p_T^{\text{lead}} = 18 - 20$  GeV (9 - 10 GeV). The uncertainties shown are from the transverse region charged  $\sum p_T$  distribution, and all the other profiles are estimated to have comparable or less systematic uncertainty. Each uncertainty is given relative to the profile value at that stage in the correction sequence and they are an average over all of the phase-space values. In the cases where the uncertainties are different for 900 GeV and 7 TeV analysis, the 900 GeV value is shown in parentheses.

Leading charged particle bin	Lowest- $p_T$	Intermediate- $p_T$	Highest- $p_T$
<b>Systematic uncertainty on unfolding</b>			
PYTHIA/PHOJET difference	4%	2%	2%
PYTHIA unfolding stat. uncertainty	< 0.1%	1% (2%)	4% (5%)
<b>Systematic uncertainties from efficiency corrections</b>			
Track reconstruction	3%	4%	4%
Leading track requirement	1%	< 0.1%	< 0.1%
Trigger and vertex efficiency	—	< 0.1% (everywhere)	—
Total from efficiency corrections	2.5%	4%	4%
<b>Systematic uncertainty for bin migration</b>			
Bin migration due to mismeasured $p_T$	-	2.5% (0%)	5% (0%)
<b>Total systematic uncertainty</b>	<b>4.5%</b>	<b>4.5% (5%)</b>	<b>8% (6.5%)</b>



## VIII. RESULTS AND DISCUSSION

### A. Overview

In this section, corrected distributions of underlying event observables are compared to model predictions tuned to a wide range of measurements. As described, the data have received minimally model-dependent corrections to facilitate model comparisons. The transverse, toward and away regions each have an area of  $\Delta\phi\Delta\eta = 10\pi/3$  in  $\eta$ - $\phi$  space, so the density of particles  $\langle d^2N_{\text{ch}}/d\eta d\phi \rangle$  and transverse momentum sum  $\langle d^2\sum p_{\text{T}}/d\eta d\phi \rangle$  are constructed by dividing the mean values by the corresponding area. The leading charged particle is included in the toward region distributions, unless otherwise stated.

The data, corrected back to particle level in the transverse, toward and away regions are compared with predictions by PYTHIA with the ATLAS MC09, DW, and Perugia0 tunes, by HERWIG+JIMMY with the ATLAS MC09 tune, and by PHOJET. The ratios of the MC predictions to the data are shown at the bottom of these plots. The error bars show the statistical uncertainty while the shaded area shows the combined statistical and systematic uncertainties. For the higher values of leading charged particle  $p_{\text{T}}$ , the data statistics are limited, so the distributions are shown only in the  $p_{\text{T}}$  range where sufficient statistics are available.

### B. Charged particle multiplicity

The charged particle multiplicity density, in the kinematic range  $p_{\text{T}} > 0.5$  GeV and  $|\eta| < 2.5$  is shown in Fig. 3 as a function of  $p_{\text{T}}^{\text{lead}}$  at  $\sqrt{s} = 900$  GeV and 7 TeV.

For the 7 TeV (900 GeV) data, the average number of charged particles in the transverse region doubles in going from  $p_{\text{T}}^{\text{lead}} = 2$  GeV(1.5 GeV) to 5 GeV (3 GeV), and then forms an approximately constant “plateau” for  $p_{\text{T}}^{\text{lead}} > 5$  GeV(3 GeV). If we assume the UE to be uniform in azimuthal angle  $\phi$  and pseudorapidity  $\eta$ , then for  $p_{\text{T}}^{\text{lead}} > 5$  GeV(3 GeV), the charged particle density of 0.8 (0.4) translates to about 5 (2.5) particles per unit  $\eta$  (extrapolating to the full  $\phi$  space) on average per event, compared to the corresponding number of  $2.423 \pm 0.001$  (stat.)  $\pm 0.042$  (syst.) ( $1.343 \pm 0.004$  (stat.)  $\pm 0.042$  (syst.)) obtained in the ATLAS minimum bias measurement [5] with  $p_{\text{T}} > 500$  MeV.

It can be concluded that the charged particle density in the underlying event, for events

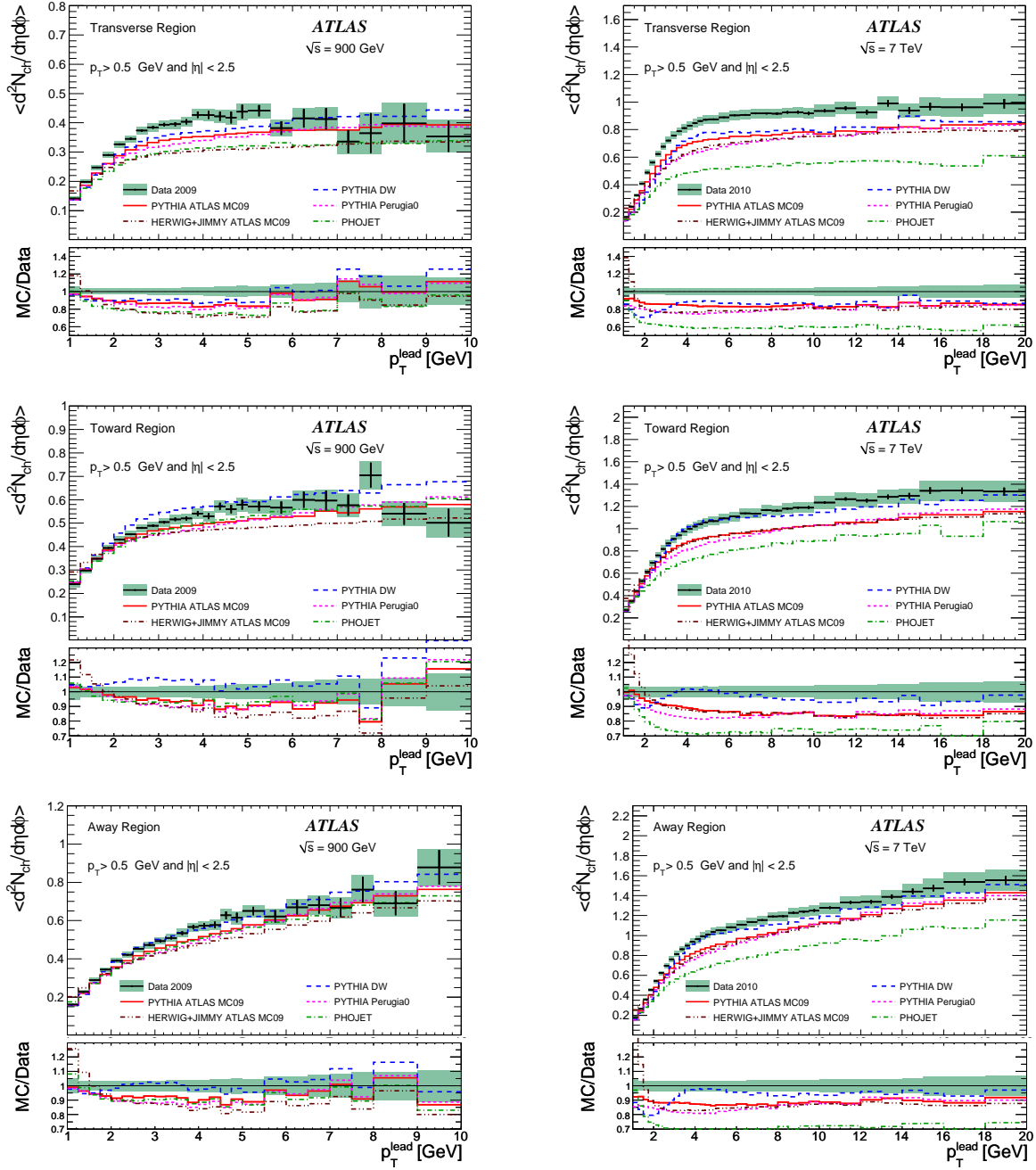


FIG. 3. ATLAS data at 900 GeV (left) and at 7 TeV (right) corrected back to particle level, showing the density of the charged particles  $\langle d^2N_{ch}/d\eta d\phi \rangle$  with  $p_T > 0.5$  GeV and  $|\eta| < 2.5$ , as a function of  $p_T^{\text{lead}}$ . The data are compared with PYTHIA ATLAS MC09, DW and Perugia0 tunes, HERWIG + JIMMY ATLAS MC09 tune, and PHOJET predictions. The top, middle and the bottom rows, respectively, show the transverse, toward and away regions defined by the leading charged particle. The error bars show the statistical uncertainty while the shaded area shows the combined statistical and systematic uncertainty.

with a leading charged particle in the plateau region (above approximately 3 or 5 GeV for the 900 GeV or 7 TeV data respectively), is about a factor of two larger than the number of charged particles per unit rapidity seen in the inclusive minimum bias spectrum. This is presumably due to the selection effect for more momentum exchange in these events, and the expected absence of diffractive contributions to the events which populate the plateau region. Given that there is one hard scattering it is more probable to have MPI, and hence, the underlying event has more activity than minimum bias.

All the pre-LHC MC tunes considered show at least 10–15% lower activity than the data in the transverse region plateau. The PYTHIA DW tune is the closest model to data for the transverse region, and in fact agrees well with the data in the toward and away regions. The most significant difference between data and MC is seen for the PHOJET generator, particularly at 7 TeV. The strong deviation of HERWIG+JIMMY from the data at low- $p_T^{\text{lead}}$  is expected, as the JIMMY model requires at least one hard scattering and therefore is not expected to be applicable in this region.

The underlying event activity is seen to increase by a factor of approximately two between the 900 GeV and 7 TeV data. This is roughly consistent with the rate of increase predicted by MC models tuned to Tevatron data. The toward and away regions are dominated by jet-like activity, yielding gradually rising number densities. In contrast, the number density in the transverse region appears to be independent of the energy scale defined by  $p_T^{\text{lead}}$  once it reaches the plateau. The 900 GeV and 7 TeV data show the same trend.

### C. Charged particle scalar $p_T$ sum

In Fig. 4 the charged particle scalar  $\sum p_T$  density, in the kinematic range  $p_T > 0.5$  GeV and  $|\eta| < 2.5$ , is shown as a function of  $p_T^{\text{lead}}$  at  $\sqrt{s} = 900$  GeV and 7 TeV.

The summed charged particle  $p_T$  in the plateau characterises the mean contribution of the underlying event to jet energies. The higher number density implies a higher  $p_T$  density as well. All the MC tunes considered show 10–15% lower  $\sum p_T$  than the data in the plateau part of the transverse region. The PYTHIA DW tune is again seen to be the closest to data in the transverse region, but it slightly overshoots the data in the toward and away regions. PHOJET is again the model furthest from the data, particularly at 7 TeV, and the strong deviation of HERWIG+JIMMY from the data at low- $p_T^{\text{lead}}$  is again expected due to

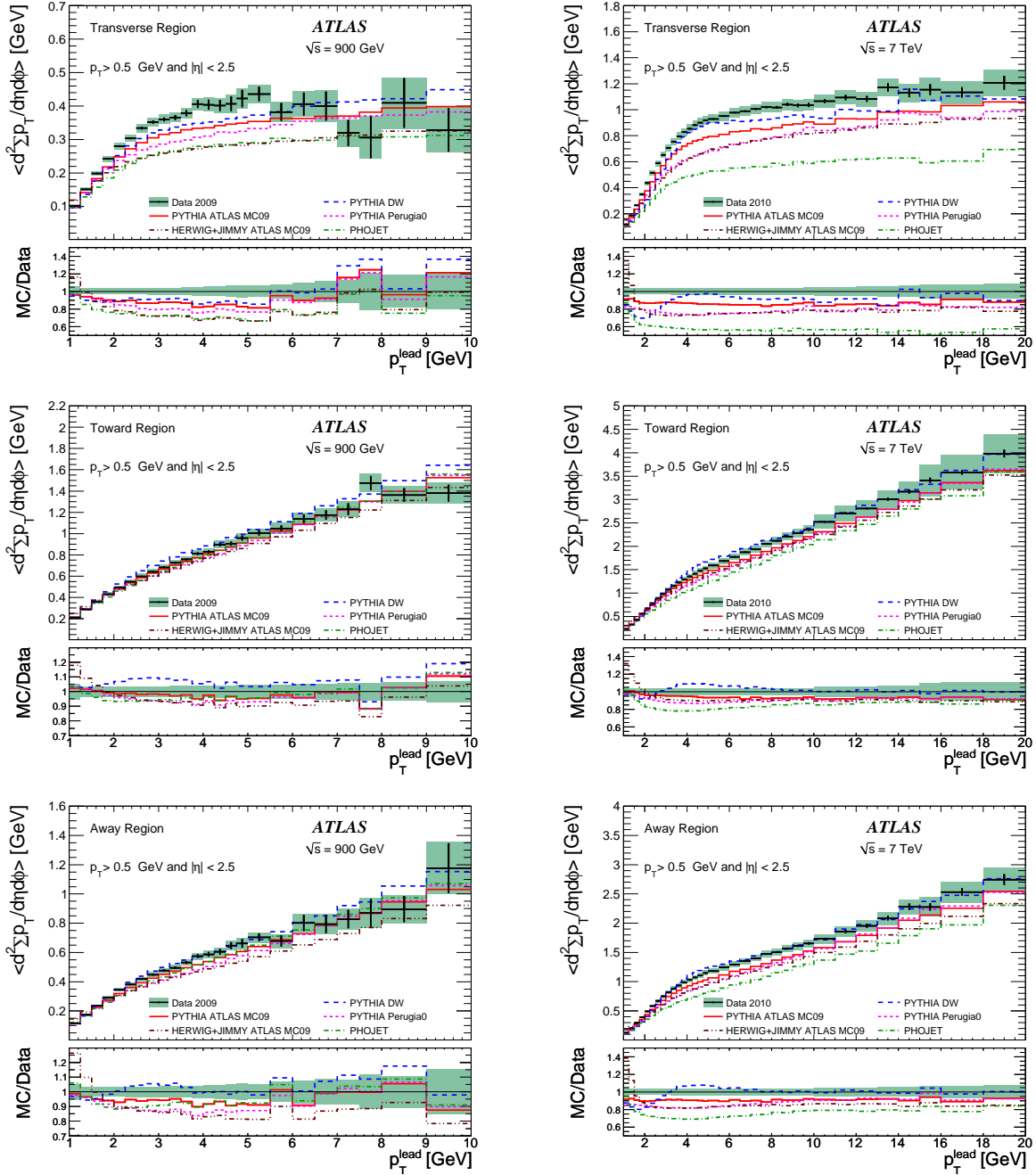


FIG. 4. ATLAS data at 900 GeV (left) and at 7 TeV (right) corrected back to particle level, showing the scalar  $\sum p_T$  density of the charged particles  $\langle d^2 \sum p_T / d\eta d\phi \rangle$  with  $p_T > 0.5$  GeV and  $|\eta| < 2.5$ , as a function of  $p_T^{\text{lead}}$ . The data are compared with PYTHIA ATLAS MC09, DW and Perugia0 tunes, HERWIG + JIMMY ATLAS MC09 tune, and PHOJET predictions. The top, middle and the bottom rows, respectively, show the transverse, toward and away regions defined by the leading charged particle. The error bars show the statistical uncertainty while the shaded area shows the combined statistical and systematic uncertainty.

the range of validity of the model. The value of  $\sum p_T$  is seen to increase by slightly more than a factor of two between 900 GeV and 7 TeV data, which is roughly consistent with the increase predicted by the MC models.

In the toward and away regions jet-like rising profiles are observed, in contrast to the plateau-like feature in the transverse region. The toward region includes the leading charged particle, and has a higher  $\sum p_T$  than the away region as there is higher probability of high- $p_T$  particles being produced in association with the leading- $p_T$  charged particle. In the toward region the highest fraction of energy has been allocated to a single charged particle. This implicitly reduces the number of additional charged particles in that region, since there is less remaining energy to be partitioned. As a result the multiplicity of charged particles is slightly lower in the toward region by comparison to the away region for high- $p_T^{\text{lead}}$ . The increase of the  $p_T$  densities in the toward and away regions indicates the extent of the variation in the charged fraction of the total energy in each region.

Multiplying the  $\sum p_T$  density by the area associated with the toward region, the  $\sum p_T$  is nearly twice what it would be if the leading charged particle were the only charged particle in the region. For the away region, the initial linear rise corresponds to the region whose total  $p_T$  nearly balances that of the leading charged particle alone. The 900 GeV and 7 TeV data show the same trend.

#### D. Standard deviation of charged particle multiplicity and scalar $\sum p_T$

In Fig. 5, the standard deviation of the charged particle multiplicity and charged particle scalar  $\sum p_T$  densities, in the kinematic range  $p_T > 0.5$  GeV and  $|\eta| < 2.5$ , are shown against the leading charged particle  $p_T$  at  $\sqrt{s} = 900$  GeV and 7 TeV (for the transverse region only).

The mean and standard deviation of the  $p_T$  density in the transverse region characterize a range of additional energy that jets might acquire if the underlying event were uniformly distributed. As the error formula is neither trivial nor particularly standard, we reproduce it here: for each bin, the sample variance of the variance of the observable  $x \in \{N_{\text{ch}}, \sum p_T\}$  is  $\text{var}(\text{var}(x)) = m_4(x) - 4 m_3(x) m_1(x) - m_2(x)^2 + 8 m_2(x) m_1(x)^2 - 4 m_1(x)^4$ , where  $m_N(x) = \langle x^N \rangle$  is the order  $N$  moment of the distribution. This is then translated into the standard error on the standard deviation of  $x$  via error propagation with a single derivative, giving symmetric errors of size  $\sqrt{\text{var}(\text{var}(x))/(n-2)} / 2\sqrt{\text{var}(x)}$ , where  $n$  is the number of entries

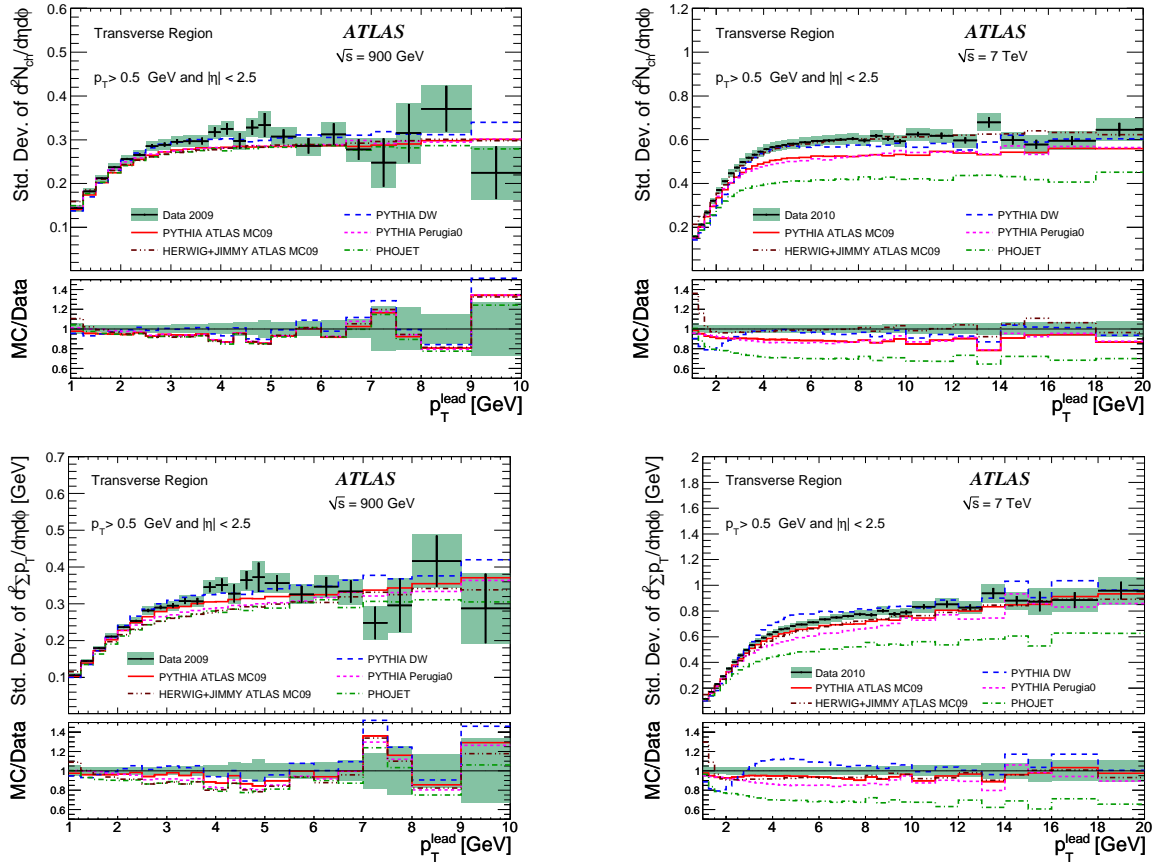


FIG. 5. ATLAS data at 900 GeV (left) and at 7 TeV (right) corrected back to the particle level, showing the standard deviation of the density of the charged particles  $\langle d^2 N_{ch}/d\eta d\phi \rangle$  (top row) and the standard deviation of the scalar  $\sum p_T$  density of charged particles  $\langle d^2 \sum p_T/d\eta d\phi \rangle$  (bottom row) with  $p_T > 0.5$  GeV and  $|\eta| < 2.5$ , as a function of  $p_T^{\text{lead}}$ , for the transverse region defined by the leading charged particle and compared with PYTHIA ATLAS MC09, DW and Perugia0 tunes, HERWIG+JIMMY ATLAS MC09 tune, and PHOJET predictions. The error bars show the statistical uncertainty while the shaded area shows the combined statistical and systematic uncertainty.

in the bin. The 900 GeV and 7 TeV data show the same trend.

The confirmation that the magnitude of the standard deviations of the distributions are comparable to the magnitudes of the mean values indicates that a subtraction of the underlying event from jets should be done on an event by event basis, rather than by the subtraction of an invariant average value. These distributions also provide an additional constraint on generator models and tunes: the discrepancy between models is much stronger at 7 TeV than at 900 GeV, with HERWIG+JIMMY giving the best description and PHOJET in particular severely undershooting the data at 7 TeV.

### E. Charged particle mean $p_T$

In Fig. 6 the average charged particle  $\sum p_T$ , in the kinematic range  $p_T > 0.5$  GeV and  $|\eta| < 2.5$ , is shown as a function of  $p_T^{\text{lead}}$  at  $\sqrt{s} = 900$  GeV and 7 TeV. These plots were constructed on an event-by-event basis by dividing the total charged particle  $p_T$  in each region by the number of charged particles in that region, requiring at least one charged particle in the considered region.

All the MC tunes, except PYTHIA tune DW, show somewhat lower mean  $p_T$  than the data in the plateau part of the transverse region and overestimate the data in the toward and away regions. The underlying event  $\langle p_T \rangle$  is seen to increase by about 20% going from  $\sqrt{s} = 900$  GeV to 7 TeV, again described by the MC models. There is relatively little discrimination between MC models for this observable, all predictions are within  $\sim 10\%$  of the data values. The toward and away regions are dominated by the jet-like rising profiles, in contrast to the plateau in the transverse region. The toward region has a higher mean  $p_T$  than the away region since there is higher probability of higher  $p_T$  particles being produced in association with the leading charged particle. The 900 GeV and 7 TeV data show the same trend.

### F. Charged particle mean $p_T$ and multiplicity correlations

The correlation between the mean  $p_T$  of charged particles and the charged particle multiplicity in each region is sensitive to the amount of hard (perturbative QCD) versus soft (non-perturbative QCD) processes contributing to the UE. This has previously been measured for inclusive minimum bias events by CDF [24] and ATLAS [5]. We present this quantity in Fig. 7 for each of the azimuthal regions in the kinematic range  $p_T > 0.5$  GeV and  $|\eta| < 2.5$ .

The profiles in the transverse and away regions are very similar, showing a monotonic increase of  $\langle p_T \rangle$  with  $N_{\text{ch}}$ . The profile of the toward region is different, as it is essentially determined by the requirement of a track with  $p_T > 1$  GeV. For  $N_{\text{ch}} = 1$ , it contains only the leading charged particle and as  $N_{\text{ch}}$  is increased by inclusion of soft charged particles the average is reduced. However, for  $N_{\text{ch}} > 5$  jet-like structure begins to form, and a weak rise of the mean  $p_T$  is observed. The 900 GeV and 7 TeV data show the same trend. Comparing

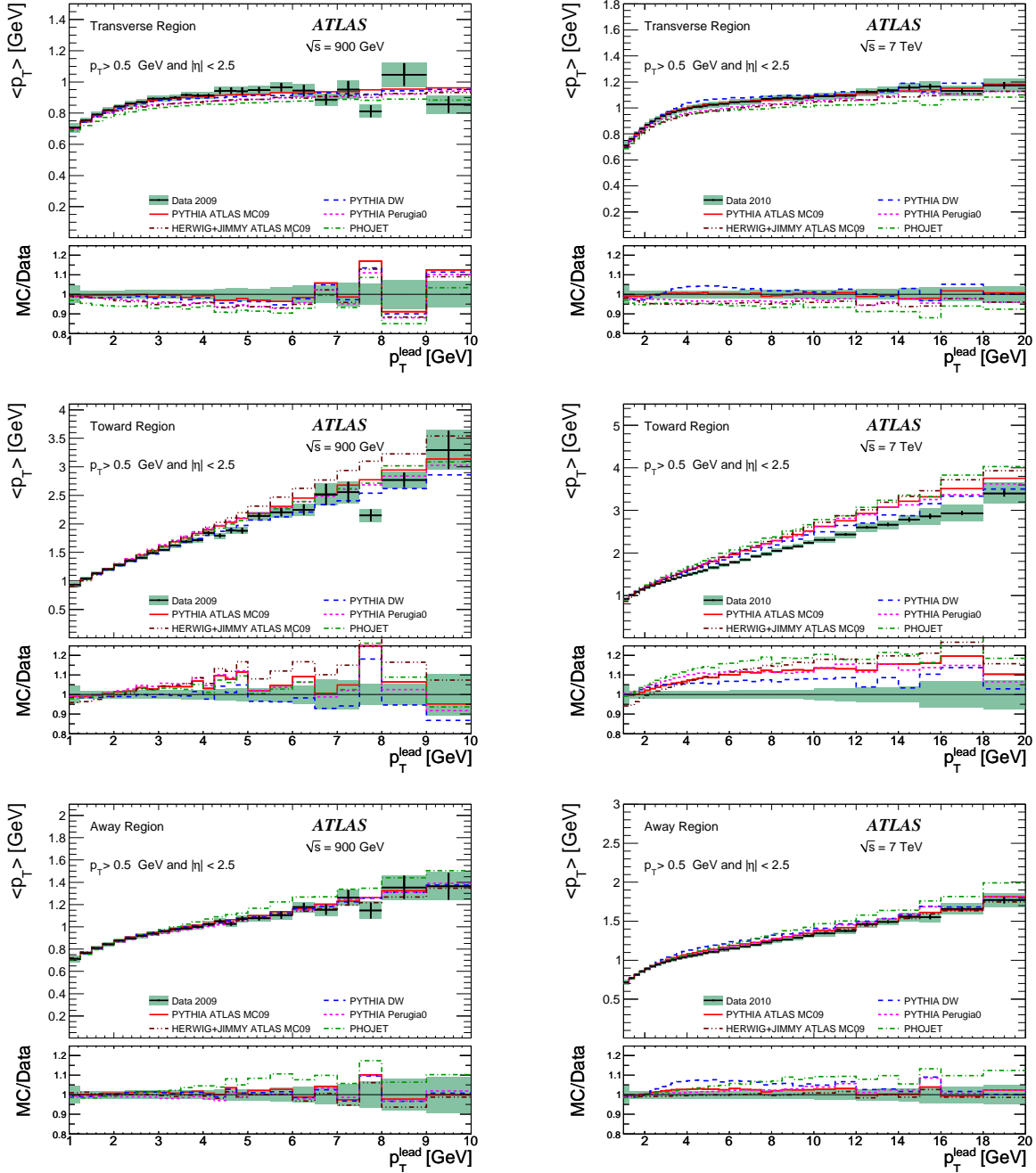


FIG. 6. ATLAS data at 900 GeV (left) and at 7 TeV (right) corrected back to particle level, showing the mean  $p_T$  of the charged particles with  $p_T > 0.5$  GeV and  $|\eta| < 2.5$ , as a function of  $p_T^{\text{lead}}$ . The data are compared with PYTHIA ATLAS MC09, DW and Perugia0 tunes, HERWIG + JIMMY ATLAS MC09 tune, and PHOJET predictions. The top, middle and the bottom rows, respectively, show the transverse, toward and away regions defined by the leading charged particle. The error bars show the statistical uncertainty while the shaded area shows the combined statistical and systematic uncertainty.



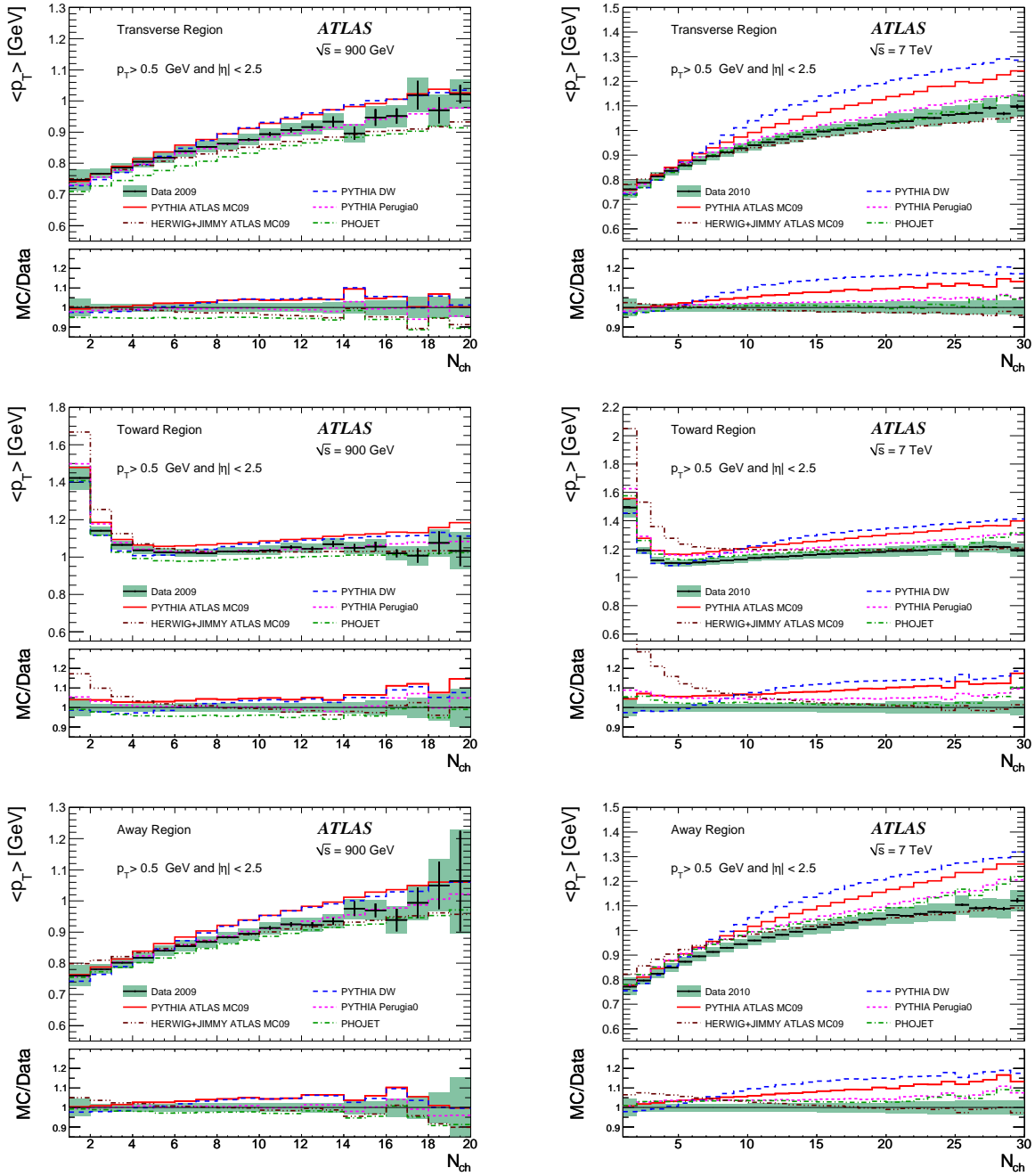


FIG. 7. ATLAS data at 900 GeV (left) and at 7 TeV (right) corrected back to particle level, showing the mean  $p_T$  of the charged particles against the charged multiplicity, for charged particles with  $p_T > 0.5$  GeV and  $|\eta| < 2.5$ . The data are compared with PYTHIA ATLAS MC09, DW and Perugia0 tunes, HERWIG + JIMMY ATLAS MC09 tune, and PHOJET predictions. The top, middle and the bottom rows, respectively, show the transverse, toward and away regions defined by the leading charged particle. The error bars show the statistical uncertainty while the shaded area shows the combined statistical and systematic uncertainty.

the 900 GeV and 7 TeV data, it is seen that the mean charged particle  $p_T$  vs.  $N_{\text{ch}}$  profiles are largely independent of the energy scale of the collisions.

The MC models again show most differentiation for the 7 TeV data, and it is interesting to see that the HERWIG+JIMMY model describes the data well at this center-of-mass energy – better than either the DW or ATLAS MC09 PYTHIA tunes (which both substantially overshoot at 7 TeV) and comparably to the Perugia0 PYTHIA tune. PHOJET gives the best description at 7 TeV. However, both HERWIG+JIMMY and PHOJET undershoot the transverse region data at 900 GeV, so no robust conclusion can be drawn about the relative qualities of the models.

### G. Angular distributions

The angular distributions with respect to the leading charged particle of the charged particle number and  $\sum p_T$  densities at  $\sqrt{s} = 900$  GeV and 7 TeV, with charged particle  $p_T > 0.5$  GeV, are plotted in Figs. 8 and 9. The leading charged particle taken to be at  $\Delta\phi = 0$  has been excluded from the distributions. The data are shown for four different lower cut values in leading charged particle  $p_T$ . These distributions are constructed by reflecting  $|\Delta\phi|$  about zero, i.e. the region  $-\pi \leq \Delta\phi < 0$  is an exact mirror image of the measured  $|\Delta\phi|$  region shown in  $0 \leq \Delta\phi \leq \pi$ .

These distributions show a significant difference in shape between data and MC predictions. With the increase of the leading charged particle  $p_T$ , the development of jet-like structure can be observed, as well as the corresponding sharper rise in transverse regions compared to the MC. The saturation at higher  $p_T$  indicates the plateau region seen in Figs. 3 and 4. PYTHIA tunes essentially predict a stronger correlation than is seen in the data, and this discrepancy in the toward region associated particle density was also observed at CDF [32].

### H. Charged particle multiplicity and scalar $\sum p_T$ for lower $p_T$ cut

In Figs. 10 and 11, the charged particle multiplicity density and charged particle scalar  $\sum p_T$  density are shown against the leading charged particle  $p_T$  at  $\sqrt{s} = 900$  GeV and 7 TeV. This time a lower  $p_T$  cut-off of 0.1 GeV is applied for the charged particles in  $|\eta| < 2.5$ .

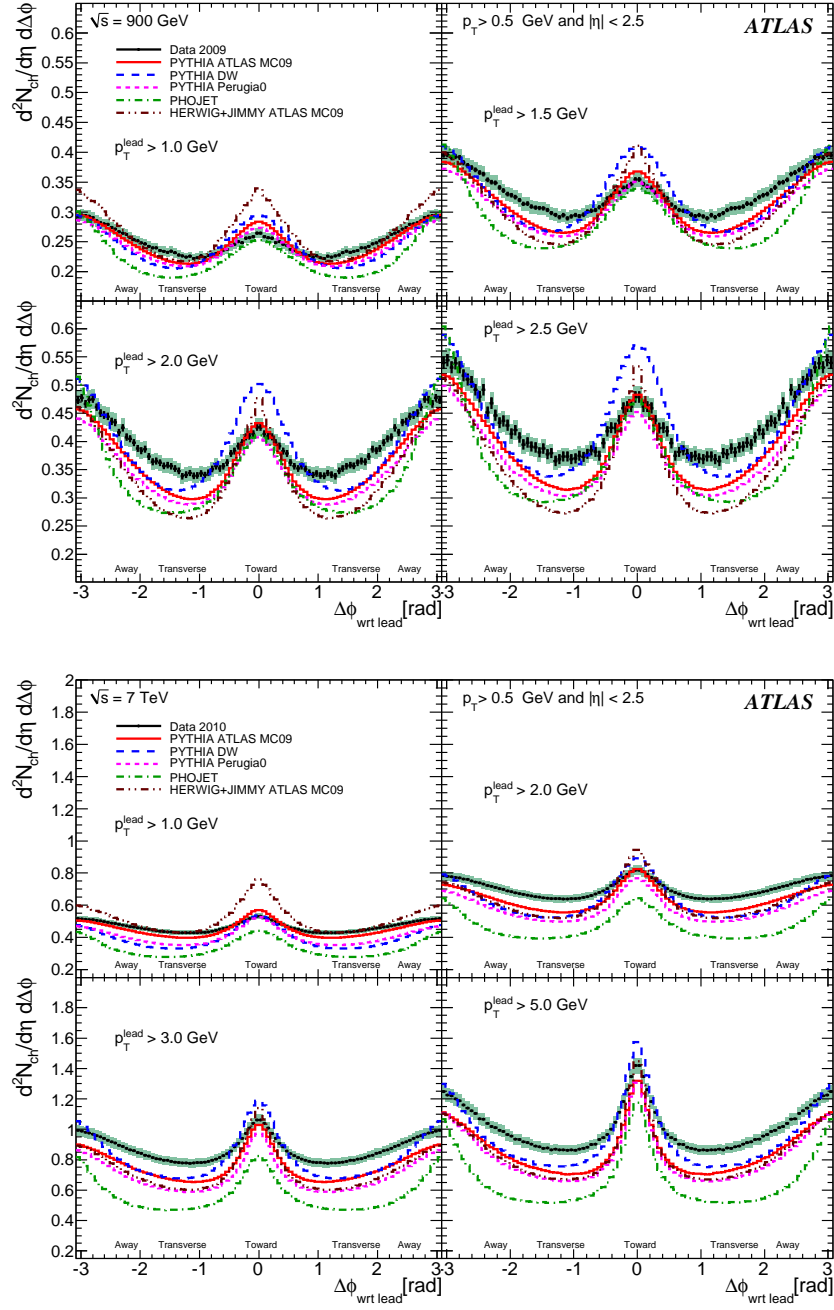


FIG. 8. ATLAS data at 900 GeV (top) and at 7 TeV (bottom) corrected back to the particle level, showing the  $\phi$  distribution of charged particle densities  $d^2N_{\text{ch}}/d\eta d\Delta\phi$  with respect to the leading charged particle (at  $\Delta\phi = 0$ ), for  $p_T > 0.5$  GeV and  $|\eta| < 2.5$ . The leading charged particle is excluded. The data are compared to MC predictions by the PYTHIA ATLAS MC09, DW and Perugia0 tunes, the HERWIG +JIMMY ATLAS MC09 tune, and PHOJET. The distributions obtained by restricting the minimum leading charged particle  $p_T$  to different values are shown separately. The plots have been symmetrized by reflecting them about  $\Delta\phi = 0$ . The error bars show the statistical uncertainty while the shaded areas show the combined statistical and systematic uncertainty corresponding to each  $p_T$  lower cut value.

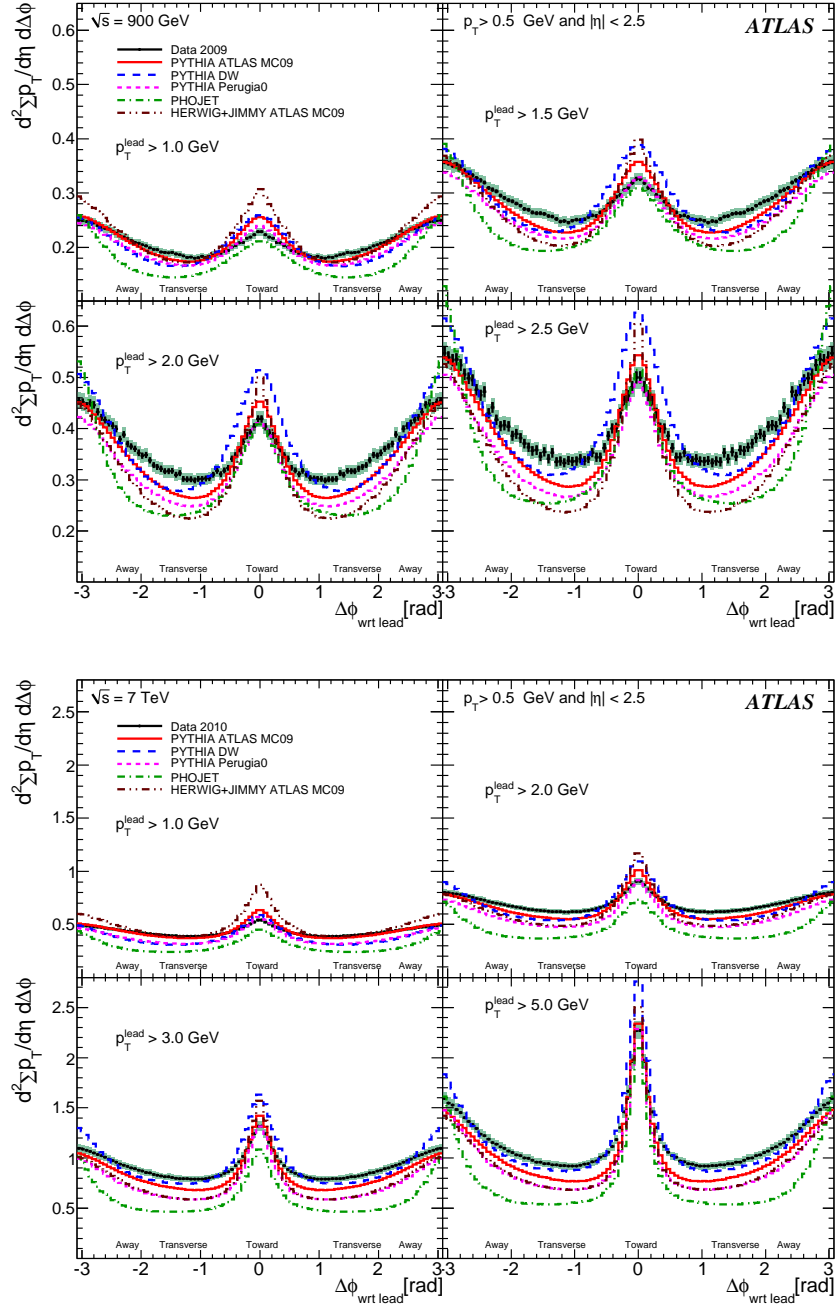


FIG. 9. ATLAS data at 900 GeV (top) and at 7 TeV (bottom) corrected back to the particle level, showing the  $\phi$  distribution of charged particle  $p_T$  densities  $d^2 p_T/d\eta d\Delta\phi$  with respect to the leading charged particle (at  $\Delta\phi = 0$ ), for  $p_T > 0.5$  GeV and  $|\eta| < 2.5$ . The leading charged particle is excluded. The data are compared to MC predictions by the PYTHIA ATLAS MC09, DW and Perugia0 tunes, the HERWIG +JIMMY ATLAS MC09 tune, and PHOJET. The distributions obtained by restricting the minimum leading charged particle  $p_T$  to different values are shown separately. The plots have been symmetrized by reflecting them about  $\Delta\phi = 0$ . The error bars show the statistical uncertainty while the shaded areas show the combined statistical and systematic uncertainty corresponding to each  $p_T$  lower cut value.

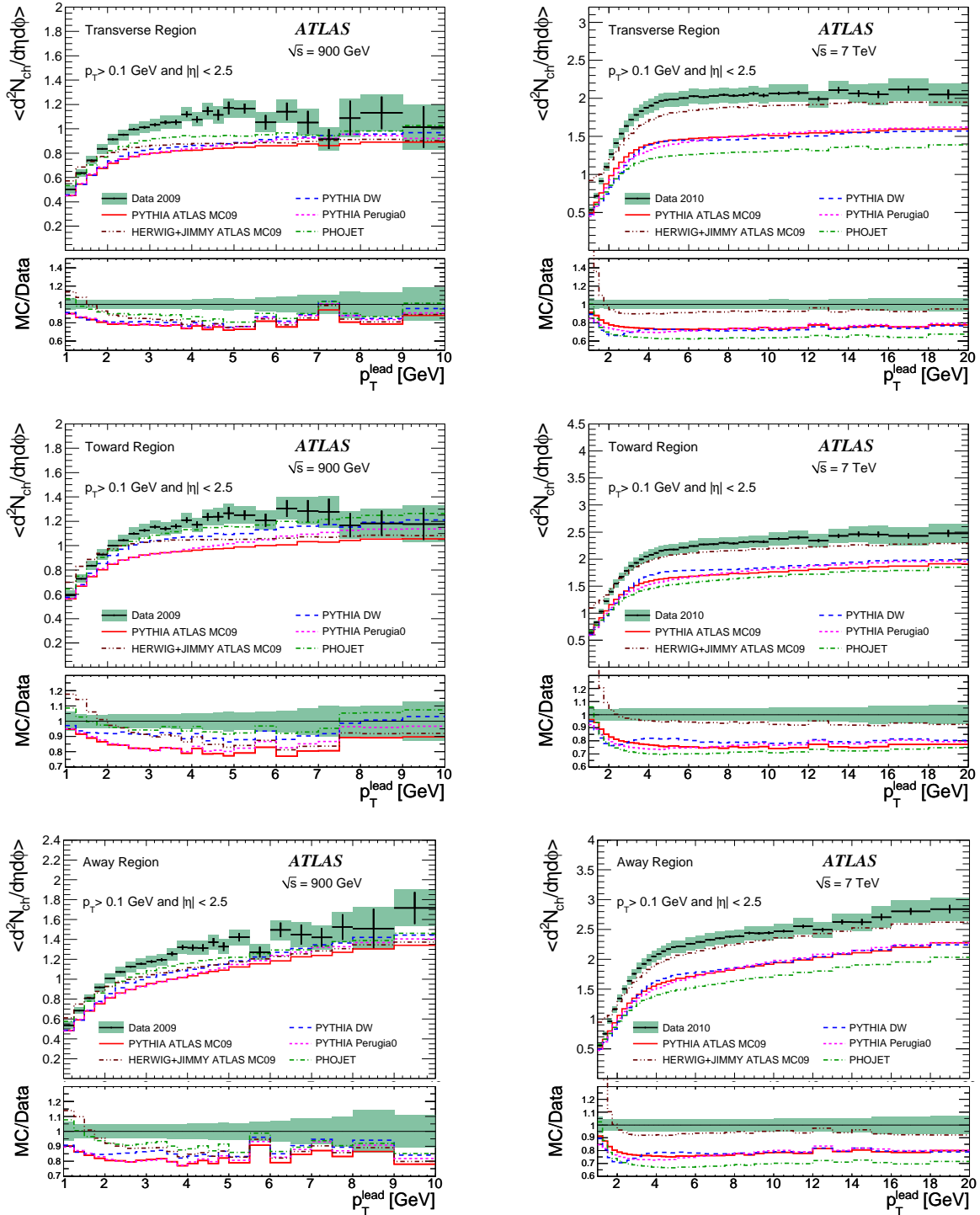


FIG. 10. ATLAS data at 900 GeV (left) and at 7 TeV (right) corrected back to particle level, showing the density of the charged particles  $\langle d^2N_{ch}/d\eta d\phi \rangle$  with  $p_T > 0.1$  GeV and  $|\eta| < 2.5$ , as a function of  $p_T^{lead}$ . The data are compared with PYTHIA ATLAS MC09, DW and Perugia0 tunes, HERWIG + JIMMY ATLAS MC09 tune, and PHOJET predictions. The top, middle and the bottom rows, respectively, show the transverse, toward and away regions defined by the leading charged particle. The error bars show the statistical uncertainty while the shaded area shows the combined statistical and systematic uncertainty.

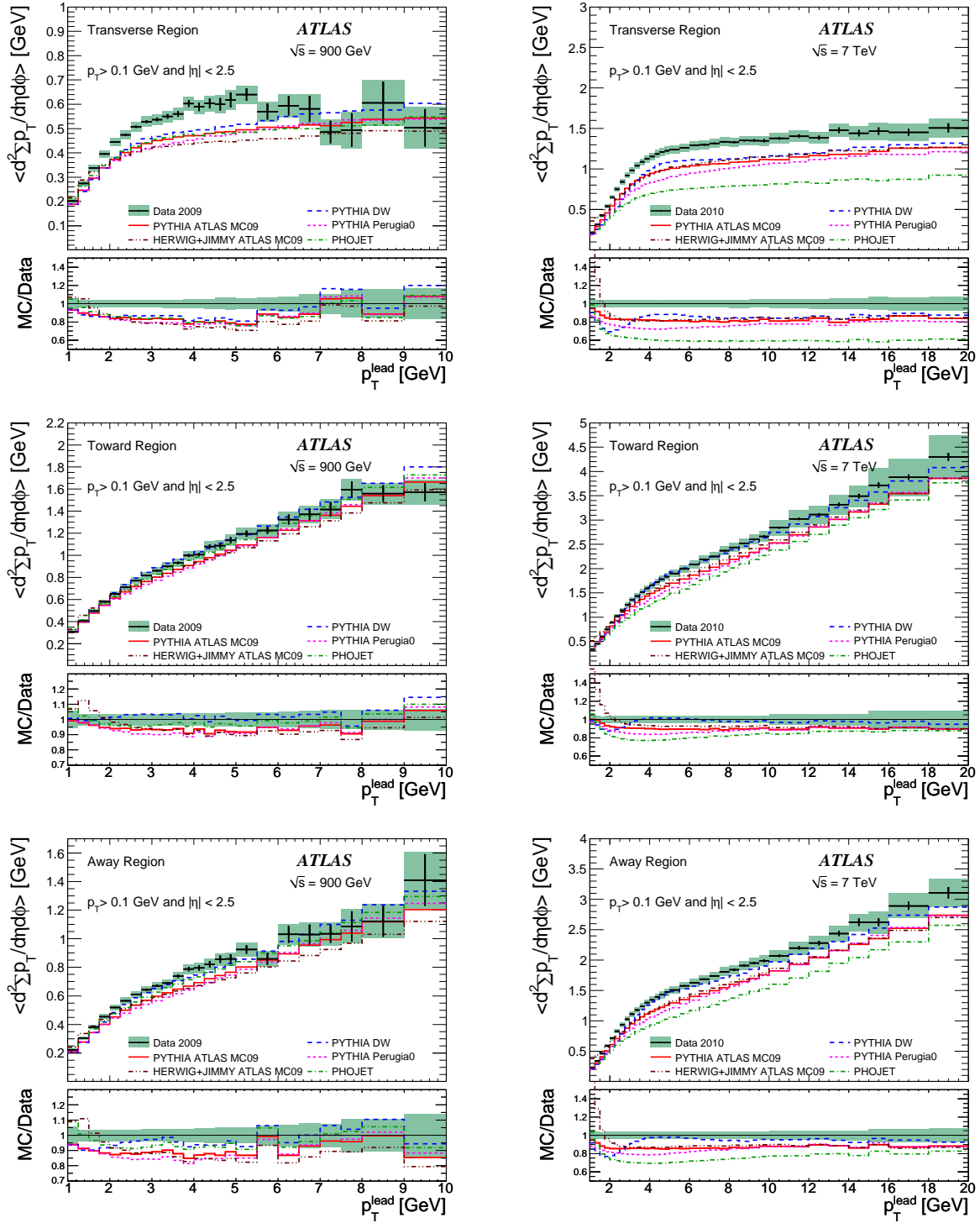


FIG. 11. ATLAS data at 900 GeV (left) and at 7 TeV (right) corrected back to particle level, showing the scalar  $\sum p_T$  density of the charged particles  $\langle d^2 \sum p_T / d\eta d\phi \rangle$  with  $p_T > 0.1$  GeV and  $|\eta| < 2.5$ , as a function of  $p_T^{\text{lead}}$ . The data are compared with PYTHIA ATLAS MC09, DW and Perugia0 tunes, HERWIG + JIMMY ATLAS MC09 tune and PHOJET predictions. The top, middle and the bottom rows, respectively, show the transverse, toward and away regions defined by the leading charged particle. The error bars show the statistical uncertainty while the shaded area shows the combined statistical and systematic uncertainty.

Compared to the previous plots with  $p_T > 500$  MeV (Figs. 3 and 4, almost a twofold increase in multiplicity is observed, but the scalar  $\sum p_T$  stays very similar. Again, the pre-LHC MC tunes show lower activity than the data in the plateau part of the transverse region, except for HERWIG+JIMMY which predicts the charged particle multiplicity density better than other models, but does not do better for the  $\sum p_T$  density. As this distinction of MC models is not seen for the  $p_T > 500$  MeV  $N_{\text{ch}}$  profile in Section VIII B, it can be seen that HERWIG+JIMMY produces more particles between 100 MeV and 500 MeV than the other MC models. A similar effect may be observed in the  $\langle p_T \rangle$  vs.  $N_{\text{ch}}$  observable of Section VIII F.

### I. Charged particle multiplicity and scalar $\sum p_T$ vs. $|\eta|$ of the leading charged particle

Figure 12 shows the charged particle multiplicity density and  $\sum p_T$  density in the kinematic range  $p_T > 0.1$  GeV and  $|\eta| < 2.5$ , for  $p_T^{\text{lead}} > 5$  GeV, against the leading charged particle pseudorapidity for  $\sqrt{s} = 7$  TeV. As this observable is composed only from events on the low-statistics transverse region plateau, the available statistics were not sufficient at  $\sqrt{s} = 900$  GeV for a robust analysis. However, the same behavior is seen as for 7 TeV.

It has been proposed that the dependence of the event characteristics on the (pseudo)rapidity can be a useful test of the centrality of the events [33]. In Fig. 12, the multiplicity and  $\sum p_T$  are seen to be independent of  $|\eta|$  for the transverse region plateau, suggesting that the average impact parameters in  $pp$  collisions do not depend strongly on  $\eta$  of the leading particle for a given  $p_T$ .

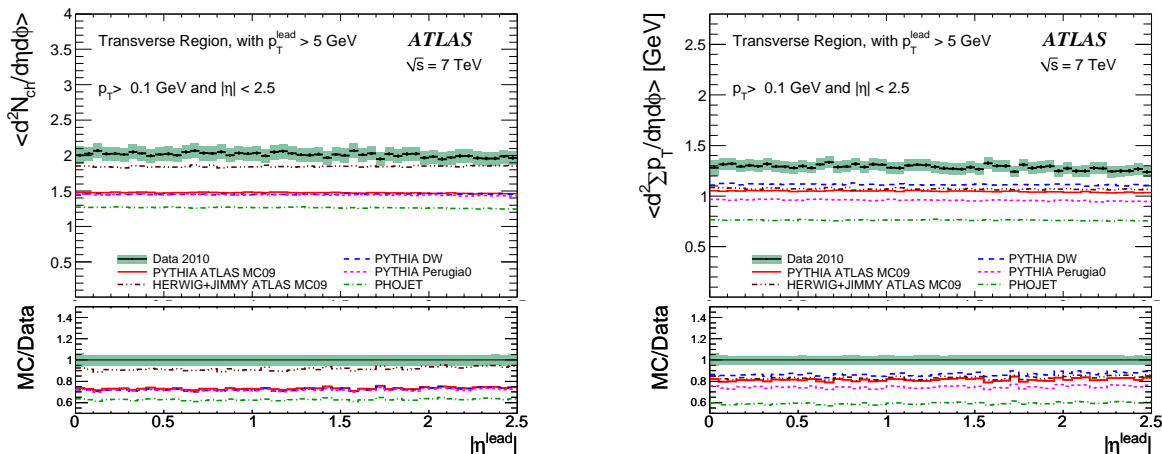


FIG. 12. ATLAS data at 7 TeV corrected back to the particle level, showing the density of the charged particles  $\langle d^2N_{ch}/d\eta d\phi \rangle$  (left) and the scalar  $\sum p_T$  density of charged particles  $\langle d^2\sum p_T/d\eta d\phi \rangle$  (right) with  $p_T > 0.1$  GeV and  $|\eta| < 2.5$ , as a function of the leading charged particle  $|\eta|$ , for the transverse region plateau ( $p_T^{lead} > 5$  GeV), defined by the leading charged particle and compared with PYTHIA ATLAS MC09, DW and Perugia0 tunes, and HERWIG+JIMMY ATLAS MC09 tune, and PHOJET predictions. The error bars show the statistical uncertainty while the shaded area shows the combined statistical and systematic uncertainty.

## IX. CONCLUSIONS

Measurements of underlying event structure with the ATLAS detector have been presented, using the data delivered by the LHC during 2009 and 2010 at center-of-mass energies of 900 GeV and 7 TeV. This is the first underlying event analysis at 7 TeV, and the first such analysis at 900 GeV to be corrected for detector-specific effects.

The data have been corrected with minimal model-dependence and are provided as inclusive distributions at the particle level. The selected phase-space and the precision of this analysis highlight significant differences between Monte Carlo models and the measured distributions. The same trend was observed for the ATLAS inclusive charged particle multiplicity measurement [4, 5]. PHOJET, HERWIG+JIMMY and all pre-LHC MC tunes of PYTHIA predict less activity in the transverse region (i.e in the underlying event) than is actually observed, for both center-of-mass energies and for charged particle minimum  $p_T$  requirements of both 100 MeV and 500 MeV. The charged particle multiplicity in the plateau of the transverse region distribution was found to be about two times higher than that of minimum bias particle density in the overall event.



One of the goals of this analysis is to provide data that can be used to test and improve Monte Carlo models in preparation for other physics studies at the LHC. The underlying event observables presented here are particularly important for constraining the energy evolution of multiple partonic interaction models, since the plateau heights of the UE profiles are highly correlated to multiple parton interaction activity. As MC models of soft physics are least predictive when modeling diffractive processes, it is particularly useful that the UE profiles are largely insensitive to contributions from soft diffraction models: the PYTHIA soft diffraction model indicates that these are constrained to the lowest bins in  $p_T^{\text{lead}}$ . However, the sensitivity to more complete diffraction models with a hard component, such as implemented in PYTHIA 8 [34] or PHOJET, has not yet been fully ascertained.

The data at 7 TeV are particularly important for MC tuning, since measurements are needed with at least two energies to constrain the energy evolution of MPI activity. While measurements from CDF exist at 630 GeV, 1800 GeV and 1960 GeV, in addition to these ATLAS measurements at 900 GeV and 7 TeV, there is a tension between the CDF and ATLAS measurements: the ATLAS analyses indicate higher levels of activity, as evidenced by the failure of MC tunes to CDF data to match the ATLAS data[35]. Hence, ATLAS UE measurement at two energies provides the best tuning data for MC predictions of ATLAS UE at higher energies. While the PYTHIA DW tune fits the ATLAS UE profile data closer than any other current tune, it fails to describe other data – as highlighted in the shape of the distribution of  $\langle p_T \rangle$  vs.  $N_{\text{ch}}$  (Fig. 7). The increase of initial state radiation activity (and different shower models) in tune DW may be responsible for this behavior. There is therefore no current standard MC tune which adequately describes all the early ATLAS data. However, using diffraction-limited minimum bias distributions and the plateau regions of the underlying event distributions presented here, ATLAS has developed a new PYTHIA tune AMBT1 (ATLAS Minimum Bias Tune 1) and a new HERWIG+JIMMY tune AUET1 (ATLAS Underlying Event Tune 1) which model the  $p_T$  and charged multiplicity spectra significantly better than the pre-LHC tunes of those generators [5, 36].

## X. ACKNOWLEDGEMENTS

We wish to thank CERN for the efficient commissioning and operation of the LHC during this initial high-energy data-taking period as well as the support staff from our institutions

without whom ATLAS could not be operated efficiently.

We acknowledge the support of ANPCyT, Argentina; YerPhI, Armenia; ARC, Australia; BMWF, Austria; ANAS, Azerbaijan; SSTC, Belarus; CNPq and FAPESP, Brazil; NSERC, NRC and CFI, Canada; CERN; CONICYT, Chile; CAS, MOST and NSFC, China; COLCIENCIAS, Colombia; MEYS (MSMT), MPO and CCRC, Czech Republic; DNRF, DNSRC and Lundbeck Foundation, Denmark; ARTEMIS, European Union; IN2P3-CNRS, CEA-DSM/IRFU, France; GNAS, Georgia; BMBF, DFG, HGF, MPG and AvH Foundation, Germany; GSRT, Greece; ISF, MINERVA, GIF, DIP and Benoziyo Center, Israel; INFN, Italy; MEXT and JSPS, Japan; CNRST, Morocco; FOM and NWO, Netherlands; RCN, Norway; MNiSW, Poland; GRICES and FCT, Portugal; MERYS (MECTS), Romania; MES of Russia and ROSATOM, Russian Federation; JINR; MSTD, Serbia; MSSR, Slovakia; ARRS and MVZT, Slovenia; DST/NRF, South Africa; MICINN, Spain; SRC and Wallenberg Foundation, Sweden; SER, SNSF and Cantons of Bern and Geneva, Switzerland; NSC, Taiwan; TAEK, Turkey; STFC, the Royal Society and Leverhulme Trust, United Kingdom; DOE and NSF, United States of America.

The crucial computing support from all WLCG partners is acknowledged gratefully, in particular from CERN and the ATLAS Tier-1 facilities at TRIUMF (Canada), NDGF (Denmark, Norway, Sweden), CC-IN2P3 (France), KIT/GridKA (Germany), INFN-CNAF (Italy), NL-T1 (Netherlands), PIC (Spain), ASGC (Taiwan), RAL (UK) and BNL (USA) and in the Tier-2 facilities worldwide.

- 
- [1] K. Aamodt *et al.* (The ALICE Collaboration), “Charged-particle multiplicity measurement in proton–proton collisions at  $\sqrt{s} = 7$  TeV with ALICE at LHC,” *Eur. Phys. J.* **C68**, 345–354 (2010), arXiv:1004.3514 [hep-ex].
- [2] K. Aamodt *et al.* (The ALICE Collaboration), “Charged-particle multiplicity measurement in proton–proton collisions at  $\sqrt{s} = 0.9$  and 2.36 TeV with ALICE at LHC,” *Eur. Phys. J.* **C68**, 89–108 (2010), arXiv:1004.3034 [hep-ex].
- [3] V. Khachatryan *et al.* (The CMS Collaboration), “Transverse momentum and pseudorapidity distributions of charged hadrons in  $pp$  collisions at  $\sqrt{s} = 0.9$  and 2.36 TeV,” *JHEP* **02**, 041 (2010), arXiv:1002.0621 [hep-ex].

- [4] G. Aad *et al.* (The ATLAS Collaboration), “Charged-particle multiplicities in  $pp$  interactions at  $\sqrt{s} = 900$  GeV measured with the ATLAS detector at the LHC,” *Physics Letters B* **688**, 21–32 (2010).
- [5] The ATLAS Collaboration, “Charged-particle multiplicities in  $pp$  interactions measured with the ATLAS detector at the LHC,” (2010), arXiv:1012.5104 [hep-ex].
- [6] T. Aaltonen *et al.* (The CDF Collaboration), “Underlying event in hard interactions at the Fermilab Tevatron  $p\bar{p}$  collider,” *Phys. Rev. D* **70**, 072002 (2004).
- [7] T. Aaltonen *et al.* (The CDF Collaboration), “Studying the underlying event in Drell-Yan and high transverse momentum jet production at the Tevatron,” *Phys. Rev. D* **82**, 034001 (2010).
- [8] V. Khachatryan *et al.* (The CMS Collaboration), “Measurement of the Underlying Event Activity in Proton–Proton Collisions at 0.9 TeV,” (2010), arXiv:1006.2083 [hep-ex].
- [9] G. Aad *et al.* (The ATLAS Collaboration), “The ATLAS Experiment at the CERN Large Hadron Collider,” *JINST* **3**, S08003 (2008).
- [10] The ATLAS reference system is a Cartesian right-handed coordinate system, with the nominal collision point at the origin. The anti-clockwise beam direction defines the positive  $z$ -axis, while the positive  $x$ -axis is defined as pointing from the collision point to the center of the LHC ring and the positive  $y$ -axis points upwards. The azimuthal angle  $\phi$  is measured around the beam axis, and the polar angle  $\theta$  is the angle measured with respect to the  $z$ -axis. The pseudorapidity is given by  $\eta = -\ln \tan(\theta/2)$ . Transverse momentum is defined relative to the beam axis.
- [11] T. Sjostrand, S. Mrenna, and P. Skands, “PYTHIA 6.4 physics and manual,” *JHEP* **05**, 026 (2006), hep-ph/0603175.
- [12] G. Aad *et al.* (The ATLAS Collaboration), “ATLAS Monte Carlo tunes for MC09,” (2010), ATL-PHYS-PUB-2010-002.
- [13] A. Sherstnev and R. S. Thorne, “Parton distributions for LO generators,” *Eur. Phys. J.* **C55**, 553–575 (2008), arXiv:0711.2473 [hep-ph].
- [14] The gluon density distribution is enhanced at low- $x$  in the modified LO\* PDF with respect to the LO CTEQ5L/6L or MSTW2008LO PDFs.
- [15] F. Abe *et al.* (The CDF Collaboration), “Transverse momentum distributions of charged particles produced in  $p\bar{p}$  interactions at  $\sqrt{s} = 630$  GeV and 1800 GeV,” *Phys. Rev. Lett.* **61**, 1819 (1988).
- [16] G. Aad *et al.* (The ATLAS Collaboration), “The ATLAS simulation infrastructure,” (2010),

- arXiv:1005.4568 [physics.ins-det].
- [17] S. Agostinelli *et al.* (The Geant4 collaboration), “Geant4: a simulation toolkit,” Nucl. Instr. Meth. **A506**, 250–303 (2003).
- [18] P. Skands, “The Perugia tunes,” (2009), arXiv:0905.3418v1 [hep-ph].
- [19] R. Field, “Min-bias and the underlying event at the Tevatron and the LHC,” A talk presented at the Fermilab MC Tuning Workshop, Fermilab (2002).
- [20] R. Engel, “Photoproduction within the two component dual parton model: Amplitudes and cross-sections,” Z. Phys. **C66**, 203–214 (1995).
- [21] G. Corcella *et al.*, “HERWIG 6.5 release note,” (2002), arXiv:hep-ph/0210213.
- [22] A. Capella *et al.*, “Jets in small- $p_T$  hadronic collisions, universality of quark fragmentation, and rising rapidity plateaus,” Phys. Lett. **B81**, 68 (1979).
- [23] A. Capella, U. Sukhatme, C-I Tan, and J. Tran Thanh Van, “Dual parton model,” Phys. Rep. **236**, 225–329 (1994).
- [24] T. Aaltonen *et al.* (The CDF Collaboration), “Measurement of particle production and inclusive differential cross-sections in  $p\bar{p}$  collisions at  $\sqrt{s} = 1.96$  TeV,” Phys. Rev. D **79**, 112005 (2009).
- [25] C. Albajar *et al.* (The UA1 Collaboration), “A study of the general characteristics of  $p\bar{p}$  collisions at  $\sqrt{s} = 0.2$  TeV to 0.9 TeV,” Nucl. Phys. **B335**, 261 (1990).
- [26] F. Abe *et al.* (The CDF Collaboration), “Pseudorapidity distributions of charged particles produced in  $p\bar{p}$  interactions at  $\sqrt{s} = 630$  GeV and 1800 GeV,” Phys. Rev. **D41**, 2330 (1990).
- [27] J. M. Butterworth, J. R. Forshaw, and M. H. Seymour, “Multiparton interactions in photoproduction at HERA,” Z. Phys. **C72**, 637–646 (1996), arXiv:hep-ph/9601371.
- [28] This is a more stringent requirement than the requirement of seven silicon hits at the track reconstruction step.
- [29] The factor of  $\sin \theta$  compensates for the  $\sin \theta$  in the denominator of the uncertainty of  $z_0$  derived from the measured distance of closest approach.
- [30] A long non-Gaussian tail in the track momentum resolution, combined with the steeply falling  $p_T$  spectrum, leads to an observed migration of very-low-momentum particles to very high reconstructed  $p_T$ , which are referred to as mismeasured tracks.
- [31] G. Aad *et al.* (The ATLAS Collaboration), “Beam parameters and machine performance to be reached in 2010,” talk presented at Evian 2010 Workshop on LHC Commissioning (2010).

- [32] R. Field, “Early QCD measurements at the LHC,” A talk presented at LHC@BNL: Joint Theory/Experiment Workshop on Early Physics at the LHC, BNL (2010).
- [33] L. Frankfurt, M. Strikman, and C. Weiss, “Transverse nucleon structure and diagnostics of hard parton-parton processes at LHC,” (2010), arXiv:1009.2559 [hep-ph].
- [34] T. Sjostrand, S. Mrenna, and P. Skands, “A brief introduction to PYTHIA 8.1,” *Comput. Phys. Commun.* **178**, 852–867 (2008), arXiv:0710.3820 [hep-ph].
- [35] The CDF measurements are within  $|\eta| < 1$ , but ATLAS measurements restricted to that  $\eta$  range show the same discrepancy as seen for the  $|\eta| < 2.5$  results presented here.
- [36] G. Aad *et al.* (The ATLAS Collaboration), “First tuning of HERWIG/JIMMY to ATLAS data,” (2010), ATL-PHYS-PUB-2010-014.